Amplitude migration in v(z) media

Oliver Lahr, Gary F. Margrave and Kay Yuhong Liu

ABSTRACT

This report is meant to investigate the notion that amplitude migration in a v(z) medium must be treated differently than migration in a constant velocity medium. It is based on findings that migrated shot gathers near edges do not show even remotely close correct amplitudes. Reasons seem to deal with the fact that geometrical, both in-phase and out of phase, must be dealt with. To prove this, a ray based analysis was undertaken to account for spreading of both kinds. Based on that, it will be shown here that accounting for a v(z) medium will result in migrations that restore amplitudes more correctly than simply assuming a constant velocity medium. In particular, we will use a flat reflector model and a simple AVO 3 model. Also, several cost-saving measures that come with this improved migration will be pointed out.

INTRODUCTION

As is well known, Kirchhoff migration works well in both depth and time domain. It has been seen to adjust for correct times and depth by a number of authors, including Bancroft (2008) and Rodriguez & Margrave (2007). However, a question has arisen how well Kirchhoff migration can preserve amplitude and what might need to be done to become a True Amplitude migration algorithm. . After some research, it was found that a number of people, including Schleicher et. al.(1993) and Zhang et. al (2000) have done work on this. They each use a different approach, of which the approach by Zhang et. al, (2000) seems to fit the pattern of the CREWES toolbox algorithms. In essence, Zhang et. al, (2000) utilize the same theory and techniques as described by (Bleistein et. al., 2001) and account for changes in v(z) media in their calculations. At this point in time, the CREWES toolbox 3D migration algorithms assume a medium with a constant speed, and utilize the Bleistein equation to implement the calculation. According to Bleistein et. al. (2001), this seems to be sufficient, however, as our previous report 'Preservation of AVO after migration' (Lahr & Margrave, 2015) indicates, this might not be the case. In that report, surveys were to be systematically decimated in order to point out qualitatively how lack of data affects final results. The surveys were 1000 x 1000 m, with shot and receiver line spacing of 10 m, 50m, 100m and 200 m respectively. As can be seen in Fig. 1.1, the results were not deemed satisfactory for the 10 m spacing, as we were expecting the migrated amplitudes to line up with the Zoeppritz curve(indicated in red). However, the 'curve' of migrated amplitudes diverges from the expected Zoeppritz result substantially. As will be seen in this report, part of the problem here is the edge effect, however, more investigation will reveal that not accounting for v(z) in the algorithm has led to this result of 'incorrect' amplitudes.

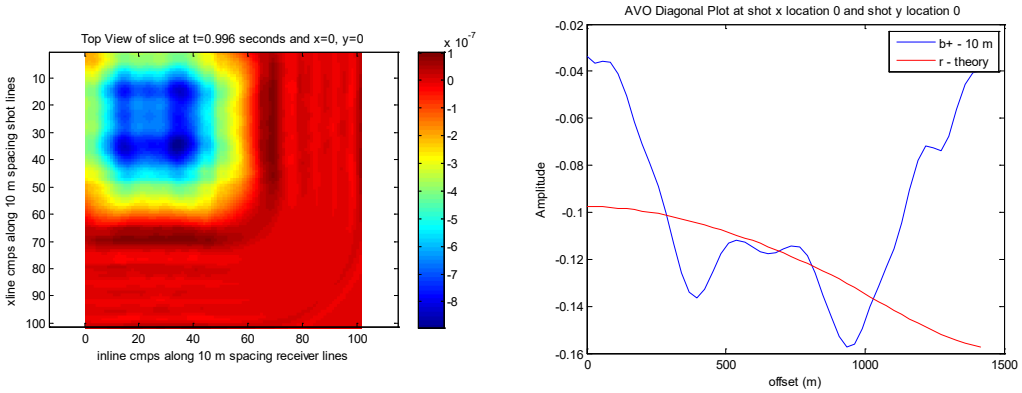

Fig. 1.1: At shot location x=y=0 on 1000m x 1000m survey a. Data slice at .996 ms for AVO 3 event b. Amplitudes at that event

The purpose of this report is to show the difference between a v(z) migration algorithm and a constant velocity one. To begin with, the main Kirchhoff migration algorithm, as pointed out by Bleistein et. al. (2001), along with a sketch of how it was derived will be shown. After that, a brief description of the constant velocity algorithms as seen in the CREWES toolbox, and its v(z) counterpart will be given. Section 4 will show the improved results of the v(z) migrations using a simple flat reflector and a simple AVO 3 reflector data set. Included in that section will be a brief discussion on edge effects will be given, after which some concluding remarks and comments about future work are made.

MIGRATION/INVERSION – THEORY

In essence, the migration utilized for this project has been derived by Bleistein et. al. (2001) for 2D, 2.5D and 3D geometries. It is valid for a generalized 3D surface as shown in Fig. 2.1, where the surface has been parameterized by $\boldsymbol{\xi}$, and the source and receivers are given by $\mathbf{x}_g$ and $\mathbf{x}_s$. The image point y will be described in further detail below.

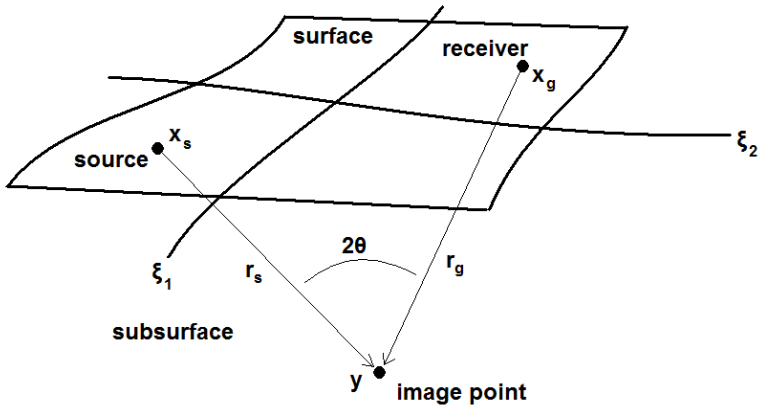

Fig. 2.1: Generalized representation of source, receiver and image point as per Bleistein et. al. (2001) – see Fig. 5.3.

It is at this image point, that the following reflectivity formula (2.1) holds true

$$\beta(\mathbf{y}) = \frac{1}{8\pi^3}\int d^2\xi \frac{|h(\mathbf{y},\boldsymbol{\xi})|}{a(\mathbf{y},\boldsymbol{\xi})|\nabla_y \emptyset(\mathbf{y},\boldsymbol{\xi})|} \cdot \int i\omega d\omega e^{-i\omega\emptyset(\mathbf{y},\boldsymbol{\xi})} u_{S(\mathbf{x}_g,\mathbf{x}_s,\omega)} \qquad (2.1)$$

where

$\beta(\mathbf{y})$ = the reflectivity at an image point **y**, i.e. some (x,y,z) point in Cartesian

Coordinates

$|h(\mathbf{y},\boldsymbol{\xi})|$= the Beylkin determinant

$a(\mathbf{y},\boldsymbol{\xi})$ = the amplitudes for both source and receivers, as per Transport equation

$\emptyset(\mathbf{y},\boldsymbol{\xi})$ = the total traveltime, as per Eikonal equation (Shearer, 1999, Appendix 3)

$u_{S(\mathbf{x}_g,\mathbf{x}_s,\omega)}$ = the scattered wavefield being inverted for, with $\mathbf{x}_g$ and $\mathbf{x}_s$ denoting the source and receiver positions

If one takes the Beylkin determinant, the amplitudes and the total travel time together, i.e.

$$\text{w}= \frac{|h(\mathbf{y},\boldsymbol{\xi})|}{a(\mathbf{y},\boldsymbol{\xi})|\nabla_y \emptyset(\mathbf{y},\boldsymbol{\xi})|} \qquad (2.2)$$

one has a amplitude weight for each point in the summation. These weights differ for 2, 2.5 and 3D shot, receiver and offset geometries and have been presented by Zhang et. al. (2002) for a v(z) velocity medium. Section 2.3 below will outline the derivation of the amplitude weight given in equation 1.2 for a 3D shot migration in a v(z) medium, while Section 2.2 will do the same for a constant velocity medium. A more complete derivation for that medium can be found in (Bleistein et al., 2001, pp. 242 – 250). For the 3D medium, Bleistein et al. (2001, Section 6.1 and 6.2) do an analougous derivation for 2.5 media.

2.1 Derivation of the Inverse Function

The inverse equation given by (2.1) arises in part due to a linearized or Born approximation of the solution (2.3) of wave scattering that have been modelled by the Helmholtz, i.e. the temporal Fourier Transform of the 3D scalar wave equation.

$$\left[\nabla^2 + \left[\frac{\omega^2}{v^2(\mathbf{x})}\right]\right] u(\mathbf{x},\boldsymbol{x_s},\omega) = -F(\omega)\delta(\mathbf{x}-\boldsymbol{x_s}) \qquad (2.3)$$

Here, the vectors **x** and $\boldsymbol{x_s}$ represent (x,y,z) locations in the 3D Cartesian coordinate system, where $\boldsymbol{x_s}$ specifically represents the source point that has caused wave propagation through a velocity medium. The speed $v(\mathbf{x})$ is known up to a given depth and unknown afterwards.. This $v(\mathbf{x})$ can be represented pictorially for the one dimensional case as seen in Figure 2.2,

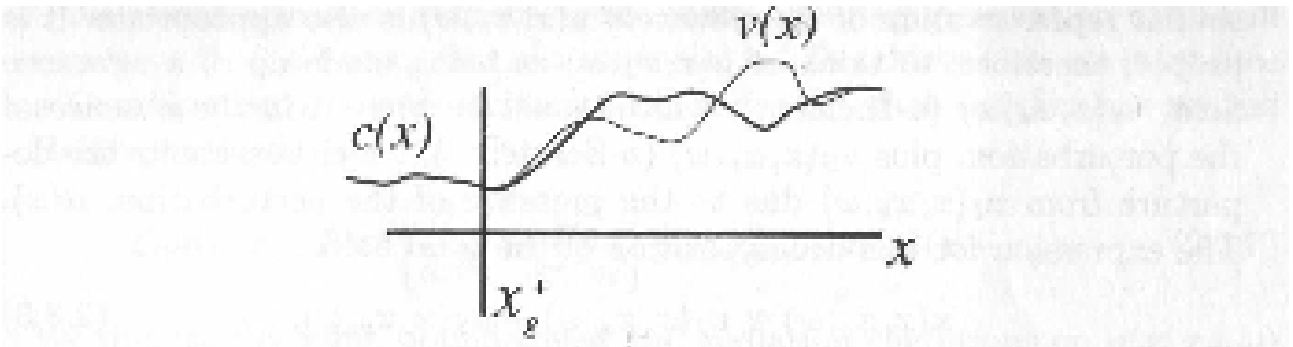

FIGURE 2.4. Cartoon showing a background wavespeed profile $c(x)$ and the actual wavespeed profile $v(x)$.

FIG. 2.2. Diagram showing background, c(x), and actual, v(x), wavespeed profile (from Bleistein et. al.(2001)).

and by equation (2.4) in 3D.

$$\frac{1}{v^2(\mathbf{x})} = \frac{1}{c^2(\mathbf{x})}\big(1 + \alpha(\mathbf{x})\big) \tag{2.4}$$

Here c(x) is the background velocity of the medium, and $\alpha(\mathbf{x})$ represents the change in speed after a given depth, i.e. at the location(s) where the wave scatters. As well, the wavefield $u(\mathbf{x}, \boldsymbol{x_s}, \omega)$ can be represented as such:

$$u(\mathbf{x}, \boldsymbol{x_s}, \omega) = u_I(\mathbf{x}, \boldsymbol{x_s}, \omega) + u_S(\mathbf{x}, \boldsymbol{x_s}, \omega) \tag{2.5}$$

where

$u_I(\mathbf{x}, \boldsymbol{x_s}, \omega)$ - represents the incident wavefield and

$u_S(\mathbf{x}, \boldsymbol{x_s}, \omega)$ - the scattered field

Knowing that the Helmholtz equation (2.5) must satisfy the Sommerfeld Radiation condition (2.6)

$$ru \text{ bounded}, r\left[\frac{\partial \mathrm{u}}{\partial r} - \frac{i\omega}{v}u\right] \to 0, as\ r \to 0, r = |\mathbf{x}| \tag{2.6}$$

a solution for the scattered wavefield, as per Bleistein et. al. (2001, p. 93) can be written as follows:

$$u_S(\mathbf{x}, \boldsymbol{x_s}, \omega) = \omega^2 \int_D \frac{\alpha(\mathbf{x})}{c^2(\mathbf{x})}[u_I(\mathbf{x}, \boldsymbol{x_s}, \omega) + u_S(\mathbf{x}, \boldsymbol{x_s}, \omega)]g\big(\mathbf{x_g}, \mathbf{x}, \omega\big)d^3x \tag{2.7}$$

Here D represents the domain of integration, and can be assumed to be the semi-infinite domain z > 0 while $g\big(\mathbf{x_g}, \mathbf{x}, \omega\big)$ represents a Green's function used to arrive at this solution. $\mathbf{x_g}$ denotes the location of the receivers.

This can be reduced to

$$u_S(\mathbf{x}, \boldsymbol{x_s}, \omega) = \omega^2 \int_D \frac{\alpha(\mathbf{x})}{c^2(\mathbf{x})} u_I(\mathbf{x}, \boldsymbol{x_s}, \omega) g(\mathbf{x_g}, \mathbf{x}, \omega) d^3x \quad (2.8)$$

for near zero-offset geometries with the help of the Born approximation, which specifies that a small $\alpha(\mathbf{x})$ will imply a small u_S for near-zero offset geometries.

Surprisingly, (2.8) also holds for arbitrary offsets, provided that we have high-frequency data. Bleistein et. al. (2001, pp 99 - 103) point this out by introducing a WKBJ trial solution for the Helmholtz equation, and deriving the eikonal and transport equations, to prove that for high frequencies the perturbation $\alpha(\mathbf{x})$ will remain small.

With this in mind, equation 2.8 can then be recast as such:

$$u_S(\mathbf{x}, \boldsymbol{x_s}, \omega) = \omega^2 F[\omega] \int_D \frac{\alpha(\mathbf{x})}{c^2(\mathbf{x})} g(\mathbf{x}, \boldsymbol{x_s}, \omega) g(\mathbf{x_g}, \mathbf{x}, \omega) d^3x \quad (2.9)$$

where $u_I(\mathbf{x}, \boldsymbol{x_s}, \omega) = F[\omega]\, g(\mathbf{x}, \boldsymbol{x_s}, \omega)$ (2.10).

Letting $(\mathbf{x}, \boldsymbol{x_0}, \omega) \sim A(\mathbf{x}, \boldsymbol{x_0}) e^{i\omega\tau(\mathbf{x}, \boldsymbol{x_0})}$, one can again follow the asymptotic derivation given by Bleistein et. al. (2001, p.220) to get the traveltime and amplitudes from $\mathbf{x}$ to $\boldsymbol{x_0}$, and rewrite (2.9) in the following manner:

$$u_S(\mathbf{x}, \boldsymbol{x_s}, \omega) \approx \omega^2 F[\omega] \int d^3x \frac{\alpha(\mathbf{x})}{c^2(\mathbf{x})} a(\mathbf{x}, \boldsymbol{\xi}) e^{i\omega\phi(\mathbf{x}, \boldsymbol{\xi})} \quad (2.11)$$

where

$a(\mathbf{x}, \boldsymbol{\xi})$ - is the product of the amplitudes contributed by the shots and receivers and

$\phi(\mathbf{x}, \boldsymbol{\xi})$ - is the total travel time from source to receiver.

The general inversion operator for (2.11) will then be

$$\alpha(\mathbf{y}) = \int d\omega \int d^2\xi B(\mathbf{y}, \boldsymbol{\xi}) e^{-i\omega\emptyset(\mathbf{y}, \boldsymbol{\xi})} u_S(\mathbf{x}_g, \mathbf{x}_s, \omega) \quad (2.12)$$

To determine $B(\mathbf{y}, \boldsymbol{\xi})$ consider that at x = y, at a partical reflection point, we have a critical point, and according to Bleistein et. al. (2001, p. 222) we can write a general solution of $\alpha(\mathbf{y})$ as such:

$$\alpha(\mathbf{y}) \sim \int d^3x \delta(\mathbf{x} - \mathbf{y})(\mathbf{x}) \quad (2.13)$$

Now, after combining (2.11) and (2.12), it can be shown that

$$\delta(\mathbf{x} - \mathbf{y}) \sim \int \omega^2 F[\omega] d\omega \int d^2\xi B(\mathbf{y}, \boldsymbol{\xi}) e^{-i\omega\{\emptyset(\mathbf{x}, \boldsymbol{\xi}) - \emptyset(\mathbf{y}, \boldsymbol{\xi})\}} \frac{a(\mathbf{y}, \boldsymbol{\xi})}{c^2(\mathbf{y})} \quad (2.14)$$

Then, doing a Taylor expansion on the phase vector

$$-i\omega\{\emptyset(\mathbf{x}, \boldsymbol{\xi}) - \emptyset(\mathbf{y}, \boldsymbol{\xi})\} \approx i\boldsymbol{k} \cdot (\mathbf{x} - \mathbf{y}) \quad (2.15),$$

where $\boldsymbol{k} \equiv \omega\nabla_y \emptyset(\mathbf{y}, \boldsymbol{\xi}) \equiv \omega\nabla_x \emptyset(\mathbf{x}, \boldsymbol{\xi})|_{x=y}$ (2.16), this leads to the forward/inverse Fourier transform like equation:

$$\delta(\mathbf{x}-\mathbf{y}) \sim \int d^3k B(\mathbf{y},\boldsymbol{\xi})\omega^2(\mathbf{k})F[\omega(\mathbf{k})]\frac{a(\mathbf{y},\boldsymbol{\xi})}{c^2(\mathbf{y})}\left|\frac{\partial(\omega,\boldsymbol{\xi})}{\partial(\mathbf{k})}\right| e^{-i\mathbf{k}\cdot\{\mathbf{x}-\mathbf{y}\}} \qquad (2.17)$$

The inverse of the Jacobian here can be rewritten as $\omega^2 h(\mathbf{y},\boldsymbol{\xi})$, where $h(\mathbf{y},\boldsymbol{\xi})$is known as the Beylkin determinant:

$$h(\mathbf{y},\boldsymbol{\xi}) = det\begin{bmatrix} \nabla_y \emptyset(\mathbf{y},\boldsymbol{\xi}) \\ \frac{\partial}{\partial \xi_1}\nabla_y \emptyset(\mathbf{y},\boldsymbol{\xi}) \\ \frac{\partial}{\partial \xi_2}\nabla_y \emptyset(\mathbf{y},\boldsymbol{\xi}) \end{bmatrix} \qquad (2.18)$$

This determinant is of paramount importance when assigning proper amplitude weights at each point in the seismic data and is the focus of the next section.

On the other hand, it can be shown that

$$B(\mathbf{y},\boldsymbol{\xi}) = \frac{1}{8\pi^3}\frac{|h(\mathbf{y},\boldsymbol{\xi})|c^2(\mathbf{y})}{a(\mathbf{y},\boldsymbol{\xi})} \qquad (2.19)$$

as the integral in (2.17) needs $F[\omega] = 1$ in order to ensure that the forward and inverse transforms behave in a correct manner. Then, accounting for band and aperture limitation, one finally arrives at (2.1). Please refer to Bleistein et. al. (2001, pp. 224-227) for a more detailed description of this derivation.

2.2 The Beylkin determinant

As mentioned in Section 2.1 above, the Beylkin determinant is of paramount importance in determining the proper amplitude weights for the inversion described by (2.1). These can be derived for common shot, common receiver and common offset surveys, in 2D, 2.5 D and 3D. Here we will only concentrate on the 3D common shot derivations, describing how these are made in a constant velocity medium and a v(z) medium.

2.2.1 The Beylkin determinant in a Common Shot medium

As shown by Bleistein et. al. (2001, Section 5.2.1 and 5.2.2), the Beylkin determinant can be written as such for a common shot inversion:

$$h(\mathbf{y},\boldsymbol{\xi}) = det\begin{bmatrix} \mathbf{p}_s + \mathbf{p}_g \\ \frac{\partial(\mathbf{p}_s+\mathbf{p}_g)}{\partial \xi_1} \\ \frac{\partial(\mathbf{p}_s+\mathbf{p}_g)}{\partial \xi_2} \end{bmatrix} \qquad (2.20)$$

where the two slowness vectors, p_s and p_g, are related to the phase term as such:

$\mathbf{p}_s = \nabla_y \emptyset(\mathbf{y},\mathbf{x}_s)$, $\mathbf{p}_g = \nabla_y \emptyset(\mathbf{x}_g,\mathbf{y})$ and $\mathbf{p}_s + \mathbf{p}_g = \nabla_y \emptyset(\mathbf{y},\boldsymbol{\xi})$.

They are also each related to the eikonal equation in the following manner

$$\mathbf{p}_S^2 = \mathbf{p}_S^2 = \frac{1}{c^2(\mathbf{y})} \tag{2.21}$$

And can each be seen to be orthogonal to the ξ_i derivatives (Bleistein et. al. 2001, p. 243).

Pictorially, these vectors are illustrated in FIG. 2.3 below, with the opening 2θ being the angle between the two vectors.

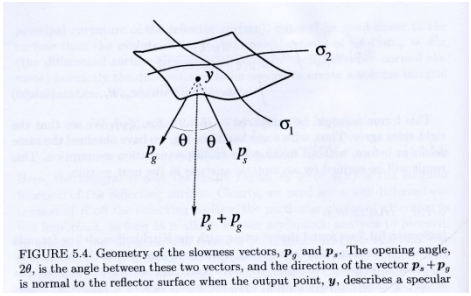

FIGURE 5.4. Geometry of the slowness vectors, $\mathbf{p}_g$ and $\mathbf{p}_s$. The opening angle, 2θ, is the angle between these two vectors, and the direction of the vector $\mathbf{p}_s + \mathbf{p}_g$ is normal to the reflector surface when the output point, $\mathbf{y}$, describes a specular

FIG. 2.3. Geometry of slowness vectors, normal to the reflector surface at point reflection point y (Bleistein et. al., p.242, Figure 5.4).

For a shot migration, (2.20) will simplify to

$$h(\mathbf{y}, \boldsymbol{\xi}) = det\begin{bmatrix} \mathbf{p}_s + \mathbf{p}_g \\ \frac{\partial \mathbf{p}_g}{\partial \xi_1} \\ \frac{\partial \mathbf{p}_g}{\partial \xi_2} \end{bmatrix} \tag{2.22}$$

as the shot at each location is held constant.

2.2.2 Constant velocity medium

Defining $c(\mathbf{y}) = constant$ and as per the derivation outlined in Bleistein et. al. (2001, Section 5.2.3), by simplifying the notation in (2.20), then expanding the Beylkin determinant as a triple scalar product, and adjusting for shot migration, it is quite easy to see that (2.1) will take the following form:

$$\beta(\mathbf{y}) = \frac{2y_3}{\pi c^2} \int d^2\xi \, \frac{r_s}{r_g^2} cos\theta \cdot \int i\omega d\omega e^{-i\omega[r_s + r_g]/c} u_{S(\mathbf{x}_g, \mathbf{x}_s, \omega)} \tag{2.23}$$

which is the form shown by Bleistein et. al. (2001, p. 247, eq. 5.2.22)

2.2.3 v(z) medium

For a v(z) medium, that is for $c(\mathbf{y})$ varying with y, revisiting the ray theoretical description of how data is generated is of paramount importance. As Bleistein et. al. (2001) and Zhang et. al (2000), among others, pointed out, in-plane and out of plane geometrical spreading needs to be accounted for when dealing with a v(z) medium.

Hence the amplitude weights as seen in (2.1) are

$$w(\mathbf{y},\boldsymbol{\xi}) = \frac{|h(\mathbf{y},\boldsymbol{\xi})|}{a(\mathbf{y},\boldsymbol{\xi})|\nabla(\tau_s+\tau_g)|^2} \tag{2.24}$$

where $\nabla(\tau_s + \tau_g)$, the gradient of the travel times, is another way of specifying $\nabla_y \emptyset(\mathbf{y},\boldsymbol{\xi})$. Note that this relates to the slowness vectors in the previous section. For a shot migration, following similar reasoning to that provided by Bleistein et. al. (2001, Section 6.1 and 6.2) for 2.5 data, it can then be shown that

$$w(\mathbf{y},\boldsymbol{\xi}) = \frac{\sqrt{cos(\alpha_{s0})}\sqrt{cos(\alpha_{g0})}}{v_0}\sqrt{\frac{\psi_s}{\psi_r}}\sqrt{\frac{\sigma_s}{\sigma_r}} \tag{2.25}$$

Here, the ψ and σ terms indicate in-plane and out-of-plane spreading for both shots and receivers respectively, the α terms are the opening and closing angles of the ray along which this set of amplitudes will be taken from and v_0 is the velocity of the first layer in the survey.

The in-plane spreading terms(shown here for the shot) are calculated as follows

$$\psi_s = cos(\alpha_s)\int_0^z \frac{v(\zeta)}{cos^3\alpha_s(\zeta)}d\zeta = cos(\alpha_s)\frac{\partial \rho_s}{\partial p_s} \tag{2.26}$$

While the out-of-plane spreading term shown here:

$$\sigma_s = \int_0^z \frac{v(\zeta)}{cos\,\alpha_s(\zeta)}d\zeta = \frac{\rho_s}{p_s} \tag{2.27}$$

The $\alpha_s(\zeta)$ terms here represent the angles at each depth point, whereas the $v(\zeta)$ values are the specific velocities at each depth point up to the depth in question.

The actual derivation, although quite straight-forward, is quite detailed and beyond the scope of this document. However, a good starting point is to look at the theory of ray tracing as described in Shearer (1999) and Krebes (2009) among others. Both sources mentioned here describe the simple ray tracing problem, starting with simple v(z) medium, showing how travel times and distances along the surfaces are calculated, before dealing with the general background for geometrical spreading.

IMPLEMENTATION OF SHOT MIGRATIONS

Although the previous discussion on arriving at the formulas for shot record migrations in a constant velocity and v(z) media have been rather detailed, the implementation is quite straight forward.

3.1 Implementation of constant velocity shot migration

This involved a simple update of the kirk_shot3D.m algorithm in the CREWES Matlab toolbox and required an outer loop for each shot, and an inner loop for all the receivers. For every inner iteration the total travel time from a shot to a receiver was determined, as were the distances, r_s and r_g traveled. The phase shifted traces were then summed together in this loop, with the correct weighting applied for every shot/receiver pair. The actual data had been phase-shifted before the loop started, to account for the data being in the frequency domain as seen by (2.23). To speed things up, summations

were done on a trace by trace basis, resulting in a total # of iterations = # of shots * # of receivers.

Note that the aperture included the entire survey, hence resulting in the total number of iterations stated here.

3.2 Implementation of v(z) Shot inversion

The same iteration will be performed for a v(z) migration. However, there will now be different weights at each location in the data, which will need to be accounted for. Also, the opening angles of each ray originating from the surface will need to be calculated. This can be done by implementing the (Chapman et. al., 1988) formulas for getting travel times and offsets per ray parameter p.(Shearer, 1999). The code for this has been implemented in the new layerext.m function in the CREWES toolbox.

Since we can never know what actual p values to use, it was decided to create a P-table that contained all offsets, in-line, x-line, times, etc. values based on the ray parameters ranging from opening angle 0 to 80 degrees. The latter angle needs to be picked to ensure that all offsets in the survey are covered. This has been implemented in createPTable.m.

The migration, i.e. inversion, can then be done in much the same manner as the migration in kirk_shot3D.m. That is, one calculates the weight for the shot to target, and iterates over all the receivers to get the weights for each ray from target location to receiver, in order to calculate the integral.

Naturally, this is incredibly time-consuming. To negate this, the P-Table was created first, as the velocity model and the survey would obviously not change. This data is then mapped to an offset table, i.e. a table which contains all the unique offsets, which is then read per offset for the loop described above. This code can be found in using createWeightsFromPTable.m. The value from this table can be loaded at runtime and can be used to update the amplitude weights at each point to be migrated. It was found that this migration performed almost as quickly as the original kirk_shot3D.m code.

3.3 Speeding up the inversion

Despite this, a migration in range of 10201 shots and receivers, with 10 m spacing between shots and shot lines, as well as receiver and receiver lines can take up to almost a week. To negate this, the kirk_shot3D.m and kirk_shot3D_vz.m codes were split to incorporate the parallel functionality of Matlab and the fact that any number of shots can be migrated at any one time. Hence, if one has a multi-processor machine, such as the CREWES Linux server, Gilgamesh, one can divide the migration across the number of workers that one has access too. Hence, if one has 10201 traces to migrate as well as 10201 receivers, as we do, and divide among 101 workers, each worker would then perform 101 migrations as described in Section 3.1 and Section 3.2. These migrated traces can then be combined and saved into some kind of persistent data storage(segy files in our case).

Now, currently, CREWES only has 96 licenses for the entire department, and these need to be used by a number of parties, however, even with 16 workers, processing times have been reduced by about 85 %, that is from about a week to about a day. More details, including the new code kirk_shot3D_par.m, for setting up the parallel implementation, and kirk_shot3D_loop.m, for doing the actual migrations on a worker, are available on request.

EXPERIMENTS AND RESULTS

To show that v(z) media cannot be correctly approximated by a migration assuming constant media, two models were created. The main one is a simplified model based on the layered model by (Zhang et. al., 2002), containing only one reflector. After that, the second model is an AVO model created with the Reflectivity method developed by Kennet (1979). It contains two layers, highlighting an AVO 3 response at 150 m. Both of these models were used to create shots at different locations in their respective surveys, which were then migrated with the constant velocity kirk_shot3D.m method, and the newly developed kirk_shot3d_vz.m code.

Slices of the results and Amplitude vs offset plots are shown to indicate to the user the differences between the algorithms. One should expect that the amplitudes for the first experiment should tend to 1, while the amplitudes for the second set of experiments should tend to their calculated AVO values.

Note also that, the model shown by Lahr and Margrave (2015) was also investigated. However, even though preliminary results, as seen in Section 4.3, look encouraging, more investigation into this more complex data set needs to be undertaken.

4.1 The Flat Layer model

This model, as mentioned, is based on the model proposed by (Zhang et. al., 2002) and derives from the model used by (Cooper, 2010). It involves placing a reflector of amplitude 1 at 150 m in a 500 m x 400 m x 400 m survey. The background velocity is 2000+0.3z, where z increases from 0 to the depth of 500 m.

Shots were created around the 400 x 400 m survey, utilizing test_shot_model3D.m in the same manner as by Cooper (2010). This involved padding the survey by 100 m on all sides, then using a WKBJ algorithm as implemented by shot_model3D.m in the CREWES toolbox. Result gathers of these shots at locations x and y = 0, 50, 100 and 200 m are shown in FIG. 4.1.

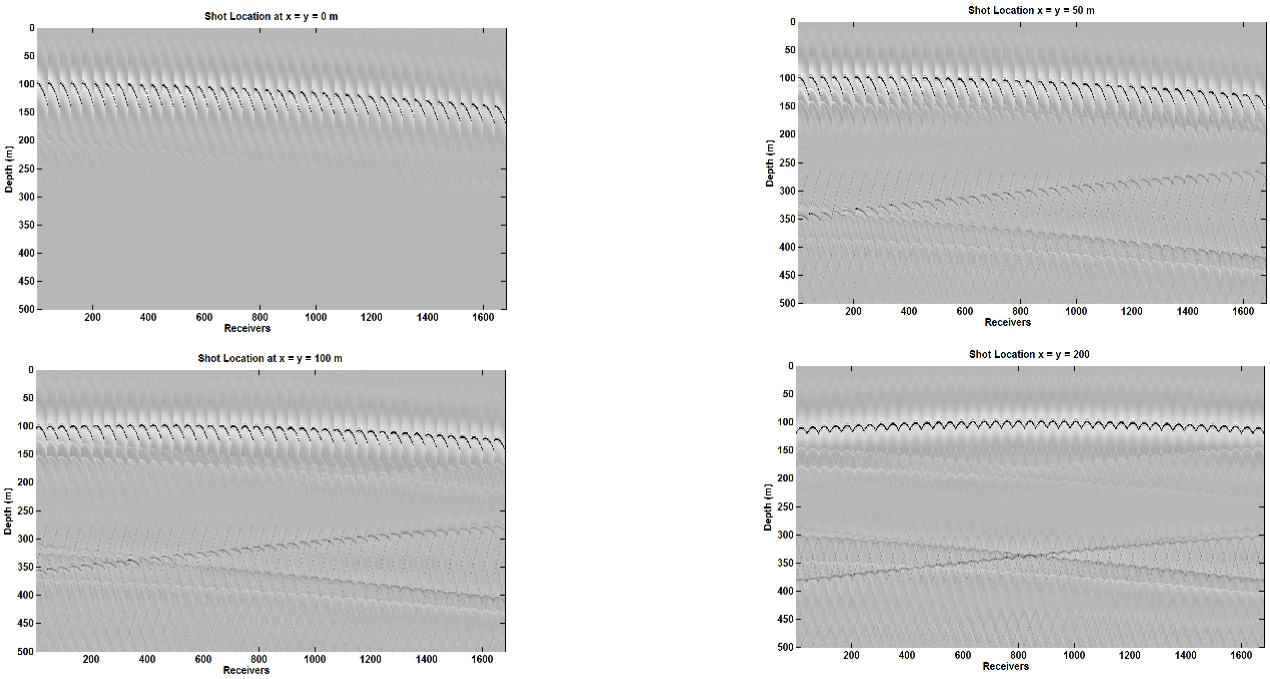

FIG. 4.1. From top left to bottom right, shot records for a flat reflector at 100 m depth in v(z) = 2000+0.3z media at location x = y = 0, 50, 100 and 200 m respectively.

These shots were then migrated with the two algorithms mentioned above, with results for all shots shown in FIG. 4.2 to 4.5.

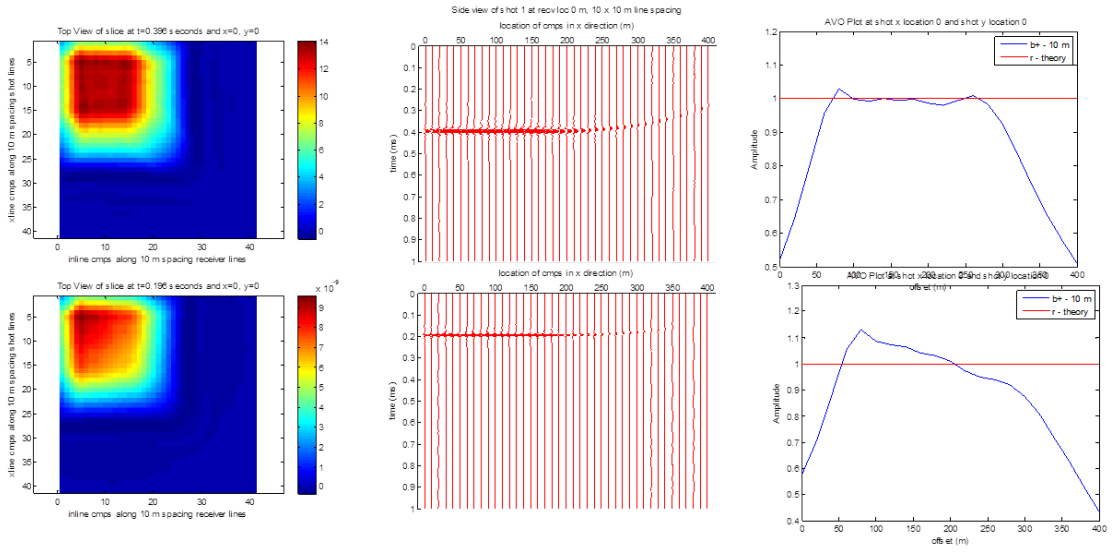

FIG. 4.2. Results of migration for flat reflector at shot location x=y = 0 m. Top Row: using v(z) algorithm Bottom Row: Using constant Kirchhoff.

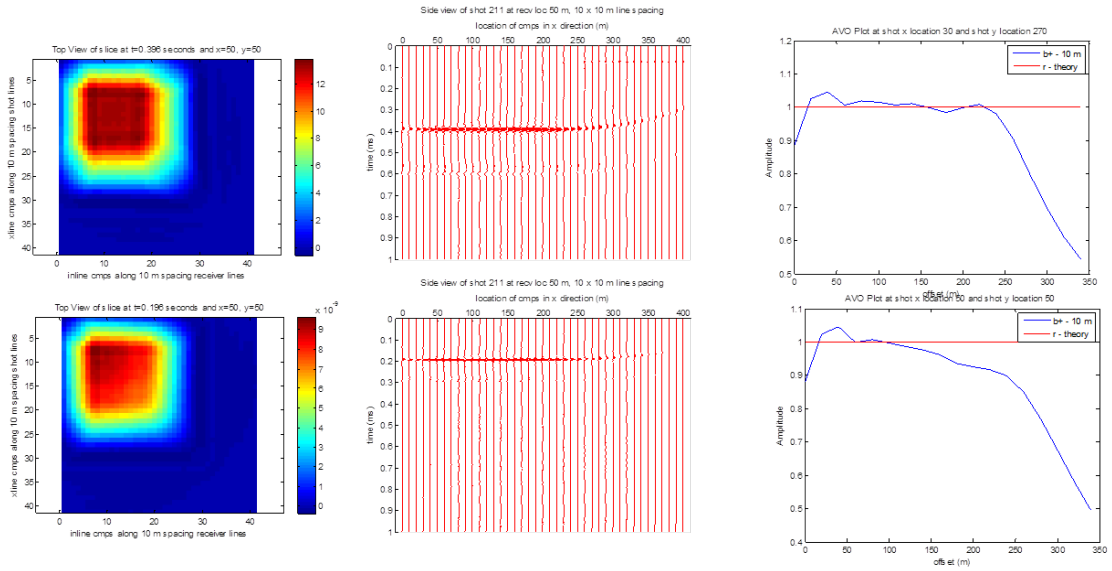

FIG. 4.3. Results of migration for flat reflector at shot location x = y = 50 m. Top Row: using v(z) algorithm Bottom Row: Using constant Kirchhoff.

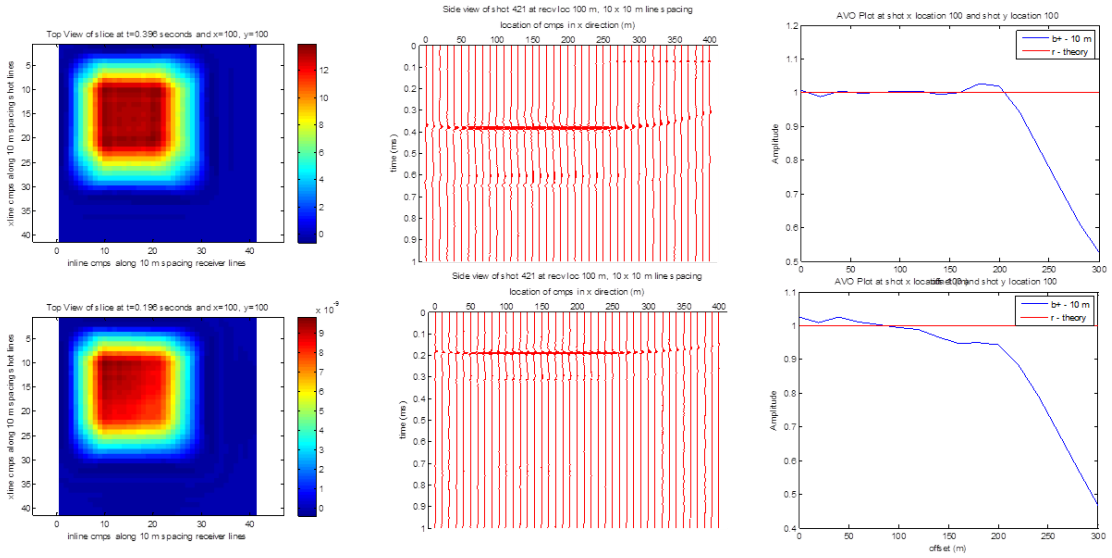

FIG. 4.4. Results of migration for flat reflector at shot location x= y = 100 m. Top Row: using v(z) algorithm Bottom Row: Using constant Kirchhoff.

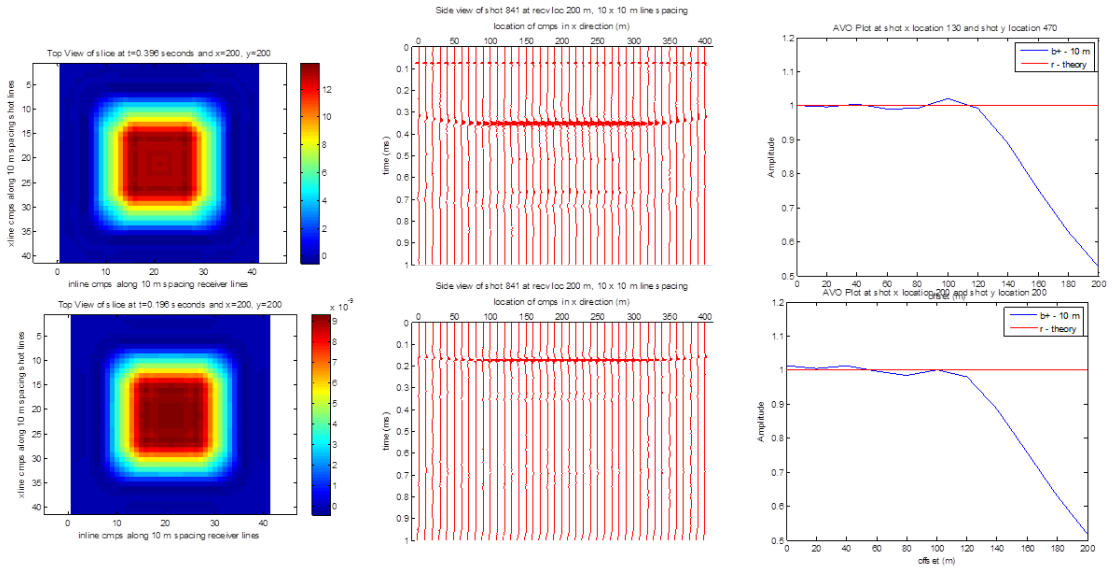

Fig. 4.5. Results of migration for flat reflector at shot location x= y = 200 m. Top Row: using v(z) algorithm Bottom Row: Using constant Kirchhoff.

As can be seen here, amplitude response is definitely better with the v(z) algorithm. Also, the amplitude response improves for both algorithms as the shots move towards the centre. However, the closer one goes to the edge, the more pronounced the edge effect becomes. This will be discussed in further detail in Section 4.4.

4.2 The Single Layer AVO Model

Before going on, note that the data created for the second, single layer AVO model being examined in this section and the more complex AVO model originally described by Lahr and Margrave (2015), dealt with in Section 4.3, were done with the Reflectivity method developed by Kennett (1979). To reiterate, this involves calculating reflection and transmission coefficients at the different boundaries in a layered half-space, and has been found to give the best seismograms for modelling purposes (Mueller, 1985). Simmons and Backus (1994) aptly point out the advantages of this method.

4.2.1 Creation of simple synthetic AVO model

As done by Lahr and Margrave (2015), the Hampson-Russell AVO modeling tool, was used to create the simple and more complex AVO model. First, a 2D synthetic seismogram was created for an upper, background layer of 300 m thickness that turns into an AVO 3 layer for the rest of the 2500 m.

The shot records for this model are shown in FIG. 4.6 for shot location x = y = 0, 50, 100, and 500 m.

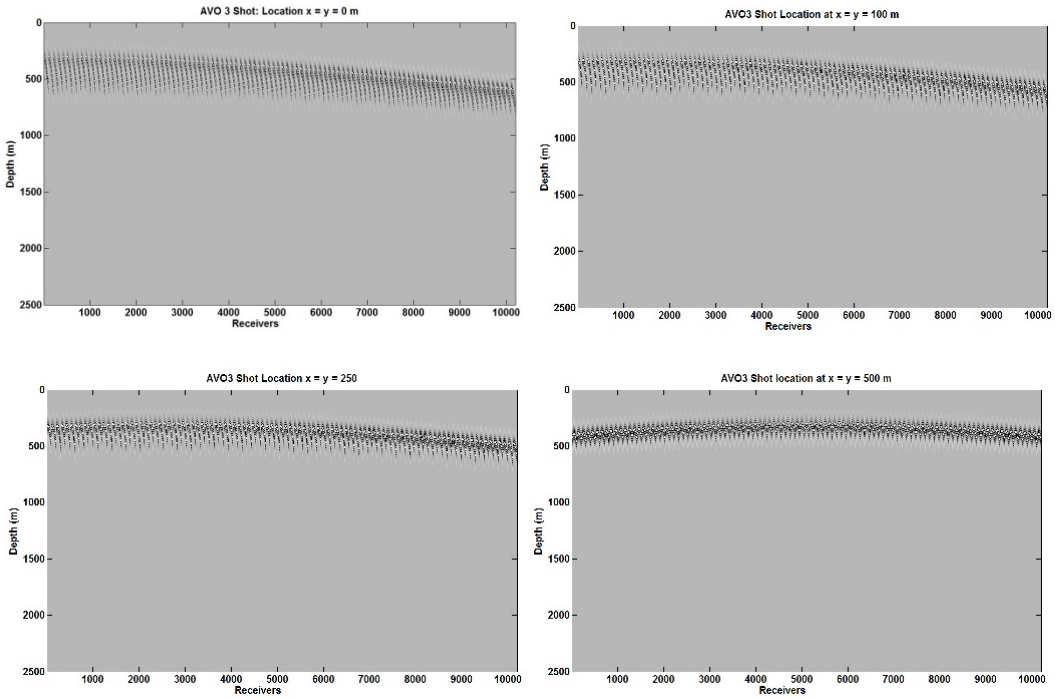

FIG. 4.6. From top left to bottom right, shot records for a AVO 3 reflector at 150 m depth at location x = y = 0, 100, 250 and 500 m respectively.

4.2.2 Results of migration for simple synthetic AVO model

These shots were also migrated with the two Kirchhoff algorithms described in Section 3, with results for shots at location x = y = 0 and 250 being shown in Figures 4.7 to 4.9.

Also, the amplitudes along the diagonal and across the receiver lines are shown in the accompanying figures (4.8 and 4.10). At this point in time, complete results for shots at (x,y) location of 100 m and 500 m are not available. However, note that preliminary data at these locations confirm the improved results(correct amplitudes) of the v(z) migration. Reasons for choosing the particular shot locations for this survey and the survey in Section 4.1 will be given in the discussion below.

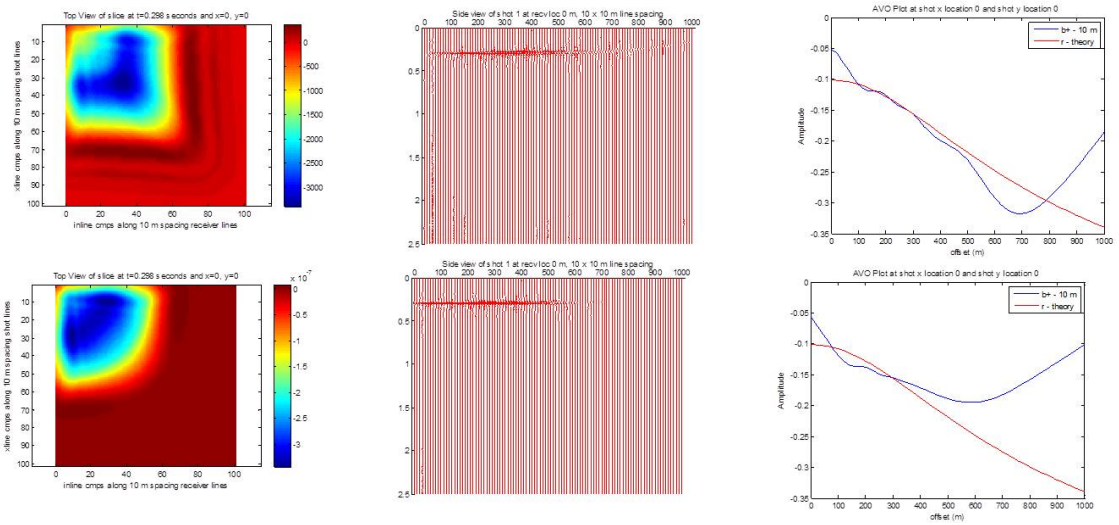

FIG. 4.7. Results of migration for Simple AVO 3 reflector at shot location x= y = 0 m. Top Row: using v(z) algorithm Bottom Row: Using constant Kirchhoff.

FIG. 4.8 is used to show that the amplitudes also fall off as expected in all directions as well with the v(z) algorithm in comparison to the v(constant) algorithm.

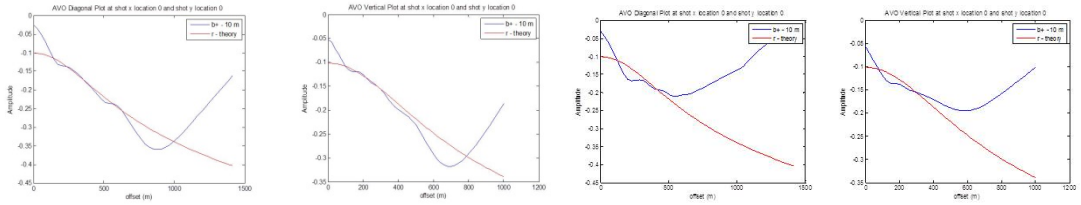

FIG. 4.8. Amplitude curves of shot at x=y=0m along a. diagonal b. along receiver line at y = 0. Left: using v(z) algorithm Right: Using constant Kirchhoff.

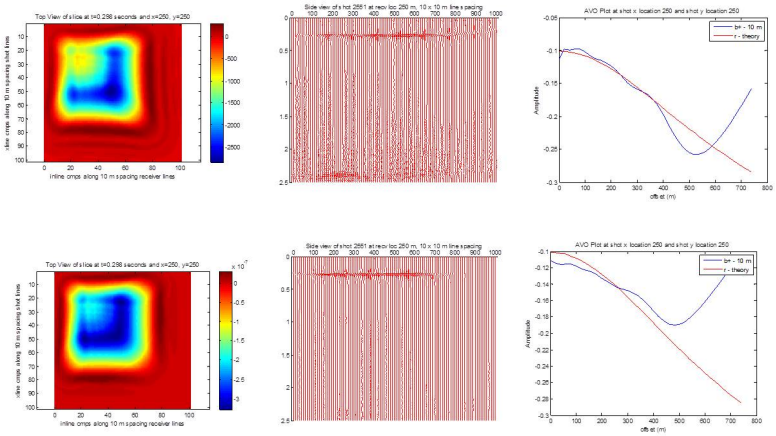

FIG. 4.9. Results of migration for Simple AVO 3 reflector at shot location x=y =250 m. Top Row: using v(z) algorithm Bottom Row: Using constant Kirchhoff.

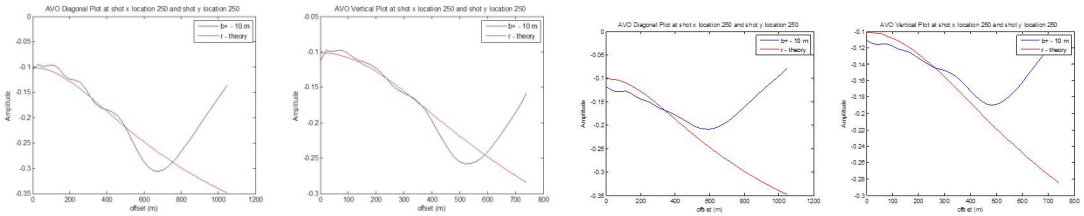

FIG. 4.10. Amplitude curves of shot at x=y=250m along a. diagonal b. along receiver line at y = 0. Left: using v(z) algorithm Right: Using constant Kirchhoff.

Again, migrations/inversions with the v(z) Kirkhoff algorithm show superior results. This is especially evident at the x = y = 250 m location, where any kind of edge effects, which will be discussed in more details in Section 4.5 have been compensated for.

4.3 The Complex, Three-Layer AVO, Model

Encouraging results were also found with the complex AVO model that was originally described by Lahr and Margrave (2015). Samples at 0 and 500 m are shown here for Event 1, which is where the background medium gives way to the AVO 3 layer at a depth of 1000 m. Remember that this layer is now 100 m thick, and will give way to the background medium at a depth of 1100 m.

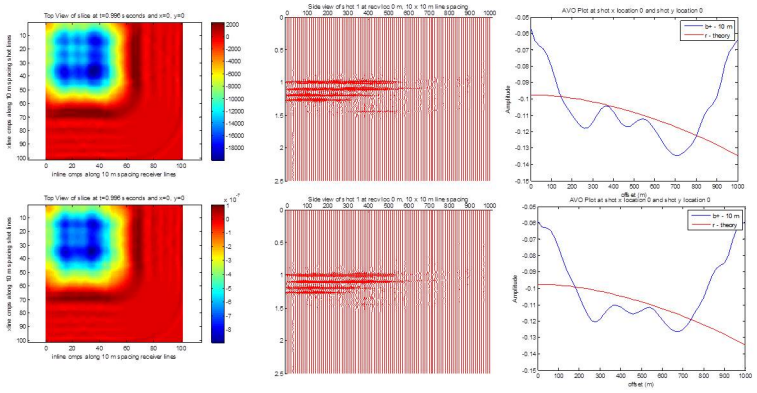

FIG. 4.15. Results of migration for Complex AVO 3 reflector at shot location x=y=0m. Top Row: using v(z) algorithm Bottom Row: Using constant Kirchhoff.

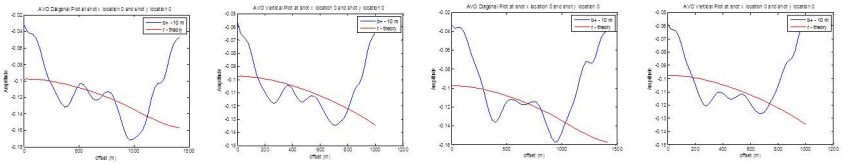

FIG. 4.16. Amplitude curves of shot at x=y=500m along a. diagonal b. along receiver line at y = 0. Left: using v(z) algorithm Right: Using constant Kirchhoff.

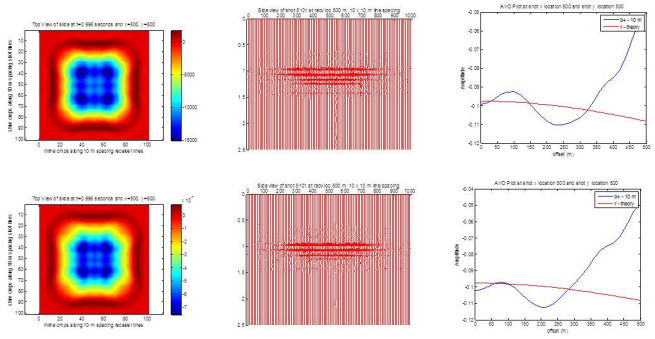

FIG. 4.17: Results of migration for Complex AVO 3 reflector at shot location x=y=0m. Top Row: using v(z) algorithm Bottom Row: Using constant Kirchhoff.

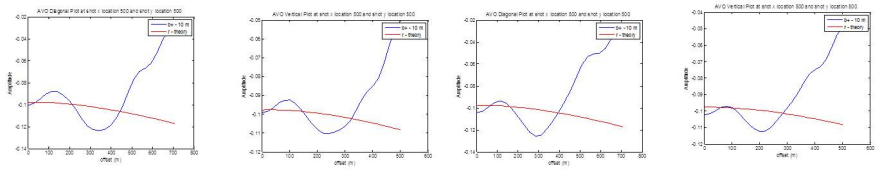

FIG. 4.18. Amplitude curves of shot at x=y=500m along a. diagonal b. along receiver line at y = 0. Left: using v(z) algorithm Right: Using constant Kirchhoff.

Surprisingly, the advantages of the v(z) migration are not as pronounced as those shown in Section 4.1 and 4.2. Most importantly, there seems to be a sinusoidal pattern in the migrated patterns. This could possibly be due to interference from the other events. But, it is quite clear that the v(z) amplitudes center along the Zoeppritz curve better than they do for the v(constant) amplitudes. Also, one can see that the edge effect is more pronounced for the v(z) algorithm. As well, the v(z) migrated amplitude seem to match the predicted amplitudes for a greater range of offsets than the constant velocity amplitudes.

Despite these advantages, and our opinion that our current v(z) migrations yield the best amplitude response, more investigation will need to be done to clarify why these results are not as good as expected.

4.4 Discussion of Results

There are several things that immediately jump out at one. First of all is that the top-left corner shot(location x=y=0m) for both the flat reflector and the simple AVO 3 reflector display a significant edge effect. Upon further investigation of the algorithm, it is easy to see that at the 0 location, only ¼ of all the traces contribute toward the final migrated point, while at the center, traces from all four quadrants of the survey add to the final result. Noting that the weights drop off the further one moves away from the image point to be migrated, one can see why there is a gap at the corner point.

Secondly, it is a bit of a surprise that the results of the v(z) migration for the complex AVO shot shown here, and in general, do not show a very significant improvement over the constant velocity migrations. However, considering that more interference is to be expected due to the proliferation of layers, this seems reasonable.

CONCLUSION AND FUTURE WORK

This report has served to show that shot record migration in a v(z) medium needs to account for the changing nature of that medium. It has been helpful in identifying some of the issues regarding amplitude preservation seen in our previous reports(Lahr and Margrave, 2015), and will aid in the actual study of that report, namely what effect does decimation have on amplitudes, even after migration. With that in mind, work is currently being done in how to carry out some advanced AVO attribute analysis with the complex AVO3 data sets presented here, which will include various degrees of decimation. Obviously, the sinusoidal nature of the migrated curves warrants investigation, but so far little information in regards to this has been found in the literature. It will definitely necessitate more research into the Kirchhoff migration presented here and amplitude preservation.

Eventually, however, further study will involve building a more complicated data model, i.e. one that gives a more realistic portrayal of a real-life seismic shoot. Also, as part of the research done here, it will be very interesting to redisplay the above amplitude plots with regards to angles instead of the offsets shown here.

ACKNOWLEDGEMENTS

We wish to thank everyone involved with the CREWES project for supporting this work.

REFERENCES

Aki, K. and P. G. Richards, 2002, Quantitative Seismology, Second Edition: University Science Books.

Bancroft, J., 2008, A practical understanding of pre- and poststack migrations: University of CalgaryCourse Notes for GOPH 659.

Bleistein, N., J. K. Cohen, and J. W. Stockwell, Jr., 2001, Mathematics of Multidimensional SeismicImaging, Migration, and Inversion: Springer.

Chapman, C.H., Jen-Yi, C. and Lyness, D.G., 1988, The WKBJ seismogram algorithm: Seismological Algorithms, Academic Press, pp. 34-371.

Cooper, Joanna K., 2010, Seismic acquisition footprint: modelling and mitigation. M.Sc. Thesis, University of Calgary.

Kennett, B., 1979, Theoretical reflection seismograms for elastic media: Geophysical Prospecting, Vol.27, p301-321.

Krebes, E.S., 2009, Geophysics 665, Lecture Notes, University of Calgary.

Lahr, O. and Margrave, G.F., 2015, Preservation of AVO after migration : CREWES Research Report, Volume 27.

Mueller, G., 1985, The reflectivity method: a tutorial: J. Geophys., 58, 153–174.

Rodriguez, Z. and Margrave, G.F., 2007, Investigation of the effects of two Kirchhoff migration algorithms on reflection amplitudes: CREWES Research Report, Volume 19.

Schleicher, J., Tygel, M., and Hubral, P., 1993, 3-D true amplitude finite-offset migration: Geophysics, 58, no.8, 1112-1126.

Shearer, Peter M., 1999, Introduction to Seismology, Cambridge University Press.

Shuey, R.T., 1985. "A simplification of the Zoeppritz equations", Geophysics, v.50, p. 609-614.

Simmons, J. L., and Backus, M., M., 1994, AVO modeling and the locally converted shear wave, Vol.59, p1237-1248.

Zhang, Y., Gray, S., and Young, J., 2000, Exact and approximate weights for Kirchhoff migration: 70th Ann. Mtg., Soc. Expl. Geophys., Expanded Abstracts, 1036-1039.

Zhang, Y., Gray, S., Cheadle, S. and Anderson, P., 2002, Factors Affecting AVO Analysis of Prestack Migrated Gathers: EAGE 64th Conference & Exhibition.

Zoeppritz, K., 1919, Erdbebenwellen VII. VIIb. Über Reflexion und Durchgang seismischer Wellen durch Unstetigkeitsflächen. Nachrichten von der Königlichen Gesellschaft der Wissenschaften zu Göttingen, Mathematisch-physikalische Klasse, 66-84.